



ELSEVIER

Contents lists available at ScienceDirect

Catalysis Today

journal homepage: www.elsevier.com/locate/cattod

Review

Preparation and characterization of bulk Mo_xC catalysts and their use in the reverse water-gas shift reaction

Xianyun Liu^{a,b}, Arturo Pajares^{a,b}, DJ Donn Calinao Matienzo^a, Pilar Ramírez de la Piscina^a, Narcís Homs^{a,b,*}

^a Departament de Química Inorgànica i Orgànica, Secció de Química Inorgànica & Institut de Nanociència i Nanotecnologia (IN2UB), Universitat de Barcelona, Martí i Franquès 1, 08028, Barcelona, Spain

^b Catalonia Institute for Energy Research (IREC), Jardins de les Dones de Negre 1, 08930, Barcelona, Spain

ARTICLE INFO

Keywords:

CO₂
CO
RWGS
Molybdenum carbides
Sol-gel method

ABSTRACT

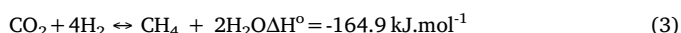
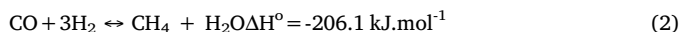
In this work, different routes for the preparation of molybdenum carbides through sol-gel methods were studied; several parameters such as molybdenum precursor, carbon source and Mo/C ratios were explored. The materials were characterized using different techniques, such as adsorption/desorption of N₂, XRD, Raman spectroscopy, SEM-EDX, TEM-EELS, H₂-TPR and XPS. Depending on the preparation method used, the presence of different Mo_xC crystalline phases, Mo₂C and/or MoC cubic and/or hexagonal, were determined. The catalytic behaviour in CO₂ conversion for CO production through the reverse water gas shift reaction was tested using a reactant mixture CO₂/H₂ = 1/3 (molar ratio) at 0.1 MPa and a gas hourly space velocity of 3000 h⁻¹. Values of CO₂ conversion up to 26 %, with nearly 100 % selectivity to CO were achieved as a function of the reaction temperature and the catalyst used.

1. Introduction

In the last years many efforts have been applied for the capture and separation of CO₂ from different effluents, because it is one of the main emissions contributing to the greenhouse effect. Nowadays CO₂ is considered an alternative C1 feedstock that can be recycled and reused in different processes [1–3]. One of the processes that is recognized useful for the CO₂ utilization is the reverse water gas shift (RWGS) reaction:



However, under RWGS conditions CH₄ can be also produced from CO or CO₂ hydrogenation:



Depending on the catalyst and the reaction conditions used, reactions (2) and (3) contribute to a decrease in the selectivity to CO of the RWGS process.

Using an appropriate catalyst, after water separation, mixtures of synthesis gas (CO₂/CO/H₂) can be obtained. These mixtures can be

used as feedstock in different industrial processes such as methanol production and Fischer-Tropsch synthesis.

Several metals have been used as active phases for the RWGS reaction, being Cu-, Ni- and noble metals-based catalysts the most studied [4–10]. One of the main problems of the use of Cu-based catalysts for the RWGS is their stability due to the sintering of the Cu active phase during the catalytic reaction [4,5]. On the other hand, Ni-based catalysts favour the methanation reaction [6] and the high cost of noble metals is an important drawback for their large scale utilization.

The similar properties of transition metal carbides (TMCs) to noble metals have led to their study as catalysts in different reactions [11,12]. In particular, TMCs are considered potential materials useful for the CO₂ activation [13,14]. The activation of CO₂ and H₂ over different model TMCs-based catalysts has been theoretically studied [15–17]. Although the most studied TMCs in CO₂ reduction have been molybdenum carbides, experimental studies have been mainly carried out using single crystal surfaces and/or at pressure higher than atmospheric [17].

Different routes have been used for the preparation of molybdenum carbides. The temperature-programmed carburization of molybdenum or molybdenum oxides, usually MoO₃, using hydrocarbon/H₂ mixtures as well as carbothermal reduction procedures have been widely applied;

* Corresponding author at: Departament de Química Inorgànica i Orgànica, Secció de Química Inorgànica & Institut de Nanociència i Nanotecnologia (IN2UB), Universitat de Barcelona, Martí i Franquès 1, 08028, Barcelona, Spain.

E-mail address: narcis.homs@qi.ub.edu (N. Homs).

<https://doi.org/10.1016/j.cattod.2019.11.011>

Received 16 January 2019; Received in revised form 10 September 2019; Accepted 12 November 2019

0920-5861/ © 2019 Elsevier B.V. All rights reserved.

these methods required careful thermal treatments at high temperatures [18–21]. Due to the increased interest in the synthesis of nano-sized carbides, new routes based in solution chemistry have been proposed. These routes enable the use of different molybdenum and carbon precursors and an interaction of the starting materials at molecular level including “soft-chemistry” pathways can take place; usually lower treatment temperature and shorter time in the preparation are involved [22–26]. We have recently reported a polycrystalline hexagonal Mo₂C highly effective in the RWGS under moderate conditions, which was prepared using a sol-gel method without carburization treatment [27]. Density functional theory (DFT) computational and experimental studies have shown that hexagonal Mo₂C has a great capability in capturing and selectively decomposing CO₂ into CO [27], the continuous O removal with H₂ can lead to H₂O formation during the RWGS. However, not all the surfaces of Mo₂C bind adsorbates with an appropriate strength; some surfaces have been theoretically shown to bind adsorbates too strongly avoiding an easy release or removal and hindering the progress of the RWGS [27]. Thus, RWGS is sensitive to the exposed Mo₂C surface. This background led us to study in the present work the RWGS over new Mo_xC-based catalysts prepared via sol-gel methods using different molybdenum precursors and carbon sources. Catalysts were characterized using N₂ adsorption/desorption isotherms, powder X-ray diffraction (XRD), scanning and transmission electron microscopy (SEM, TEM), temperature programmed reduction with H₂ (H₂-TPR), X-ray photoelectron spectroscopy (XPS) and Raman spectroscopy. The catalytic behaviour in the RWGS was analysed as a function of the characteristics of the catalysts which in turn depended on the preparation method used. Moreover, for the more performant catalyst, a long-time catalytic test, to verify its stability and catalytic behaviour, was carried out.

2. Experimental

2.1. Preparation of catalysts

Different Mo_xC catalysts were prepared using sol-gel methods and different Mo precursors and carbon sources. MoCl₅ or (NH₄)₆Mo₇O₂₄·4H₂O were used as Mo precursor; three different sources of carbon were used: urea, a mixture of citric acid and urea in the presence of ethylene glycol (EG), a mixture of ethylenediaminetetraacetic acid (EDTA) and ethylenediamine (ED), sucrose, and, 4,5-dicyanoimidazole (DI). In all cases, the Mo precursor was mixed with the carbon source in water or ethanol to form a viscous solution. The viscous solution was then treated at 333 K for 48 h in an oven under air to form a gel. After this, the sample was transferred into a tubular quartz reactor, treated under Ar flow (20 mL min⁻¹) at 2 K min⁻¹ up to 423 K and maintained 3 h. Subsequently, the temperature was increased at 3 K min⁻¹ up to 1073 K and kept 3 h. Finally, the reactor was cooled down to room temperature under Ar flow and the catalyst was exposed to the

ambient air without passivation. Table 1 shows metal precursor, carbon source and the carbon source/metal precursor ratio used for the preparation of catalysts labelled: Mo_xC-A [27], Mo_xC-B, Mo_xC-C, Mo_xC-D, Mo_xC-D1 and Mo_xC-E. Additional experimental details for the preparation of the catalysts are given in the Supporting Information.

2.2. Characterization of catalysts

N₂ adsorption-desorption isotherms were recorded at 77 K using a Micromeritics Tristar II 3020 equipment. Prior to the measurements, the samples were outgassed at 523 K. The surface area (S_{BET}) was calculated by multi-point B.E.T. analysis of nitrogen adsorption isotherms. XRD patterns were obtained with a PANalytical X'Pert PRO MPD Alpha1 powder diffractometer equipped with a CuKα₁ radiation. The XRD profiles were collected between 2θ = 4° and 2θ = 100°, with a step width of 0.017° and by counting 50 s at each step.

Raman spectroscopy analyses were registered using a Jobin-Yvon LabRam HR 800, fitted to an optical Olympus BXFM microscope with a 532 nm laser and a CCD detector. The Raman spectra of the samples were collected with laser power limited to 1.5 mW to minimize laser-heating effects. H₂-TPR experiments were performed using a Micromeritics AutoChem II 2920 chemisorption analyser. Approximately 50 mg of sample was pretreated at 363 K under flowing He. After cooling to room temperature, the sample was exposed to a H₂/Ar (12 % v/v) flow, and the temperature was linearly increased at 10 K min⁻¹ up to 1073 K.

SEM analysis was carried out in a JEOL J-7100 F microscope working with an electron acceleration potential of 20 kV and equipped with an energy dispersive X-ray (EDX) detector. The EDX analysis was performed with an Oxford Instrument INCA at an acquisition time of 60 s. TEM images and electron energy loss (EEL) spectra were acquired in a JEOL 2010 F microscope, equipped with a field emission electron gun working with an electron acceleration potential of 200 kV and coupled to a Gatan imaging filter.

The XPS were obtained in a PerkinElmer PHI-5500 Multitechnique System equipment with an Al X-ray source (hν = 1486.6 eV and 350 W). All measurements were carried out in an ultrahigh vacuum chamber (P < 2 × 10⁻⁸ Torr). The binding energy (BE) values were referred to the C 1s BE of adventitious carbon at 284.8 eV, which was previously determined in the same equipment and conditions, using Au as reference.

2.3. Catalytic tests

The RWGS reaction tests were carried out using a tubular fixed-bed reactor (316-L stainless steel, 305 mm long, 9 mm i.d.) provided with a thermocouple in direct contact with the catalyst in a Microactivity-Reference unit (PID Eng&Tech). The catalyst sample, approximately 150 mg, was diluted with silicon carbide up to 1 mL. Catalyst was firstly

Table 1
Several parameters of Mo_xC preparation and S_{BET} values and crystallite size (determined by XRD) of Mo_xC.

Catalyst	Metal precursor	Carbon source	mol Carbon source/mol Metal precursor	S _{BET} (m ² g ⁻¹)		Crystallite size (nm)
				Fresh	Used	
Mo _x C-A	MoCl ₅	urea	7	8	5	35.2
Mo _x C-B	(NH ₄) ₆ Mo ₇ O ₂₄ ·4H ₂ O	urea + EG ¹ + CA ²	urea,7; EG,7; CA,7	15	11	12.2
Mo _x C-C	(NH ₄) ₆ Mo ₇ O ₂₄ ·4H ₂ O	EDTA ³ + ED ⁴	EDTA, 3.5; ED,7	9	–	4.6
Mo _x C-D	(NH ₄) ₆ Mo ₇ O ₂₄ ·4H ₂ O	sucrose	12	< 5	< 5	3.3
Mo _x C-D1	(NH ₄) ₆ Mo ₇ O ₂₄ ·4H ₂ O	sucrose	6.6	< 5	< 5	20.6
Mo _x C-E	MoCl ₅	⁵ DI	0.5	18	28	25.0

¹ EG: Ethylene glycol.

² CA: Citric acid.

³ EDTA: Ethylenediaminetetraacetic acid.

⁴ ED: Ethylenediamine.

⁵ DI: 4,5-dicyanoimidazole.

treated under N_2 flow from 298 K up to 598 K for 3 h. Then, the reactant $CO_2/H_2/N_2 = 1/3/1$ mixture, under a gas hourly space velocity (GHSV) of 3000 h^{-1} , was introduced. The RWGS was studied at 0.1 MPa, between 548 K and 673 K, following the temperature sequence: 598 K (3 h) \rightarrow 573 K (3 h) \rightarrow 548 K (10 h) \rightarrow 598 K (3 h) \rightarrow 623 K (3 h) \rightarrow 648 K (3 h) \rightarrow 673 K (3 h) \rightarrow 648 K (5 h). An additional long-term catalytic test of about 100 h on stream at 623 K, was carried out over the Mo_xC -B, which was the most performant catalyst. The reactor effluent was analysed on-line with a Varian 450-GC equipped with a methanizer, a TCD and two FID detectors. The system was allowed to stabilize at each temperature at least for 1 h before the analysis, which was performed twice. The corresponding blank tests with the empty reactor and with SiC showed a negligible contribution to the reaction under the experimental conditions used.

3. Results and discussion

As stated before, catalysts prepared in this work are shown in Table 1; the preparation and characterization of Mo_xC -A has been recently reported [27]. All catalysts have low values of BET surface-area (Table 1), being the highest that of Mo_xC -E ($18\text{ m}^2\text{ g}^{-1}$). XRD diffraction patterns (Fig. 1) indicate the presence of different Mo_xC phases with different crystallinity degree as a function of the preparation method used. XRD patterns of Mo_xC -A, Mo_xC -D1 and Mo_xC -E clearly show peaks corresponding to hexagonal Mo_2C (JCPDS 00-035-0787) with high crystallinity. In all the other catalysts, the presence of hexagonal Mo_2C with lower crystallinity can be proposed. On the other hand, the presence of a wide peak at $2\theta = 36\text{--}39^\circ$ and the absence of a peak at $2\theta = 48.8^\circ$ could be related with the presence of cubic Mo_2C (JCPDS 00-015-0457) and/or MoC (JCPDS 03-065-0280) in Mo_xC -B, Mo_xC -C,

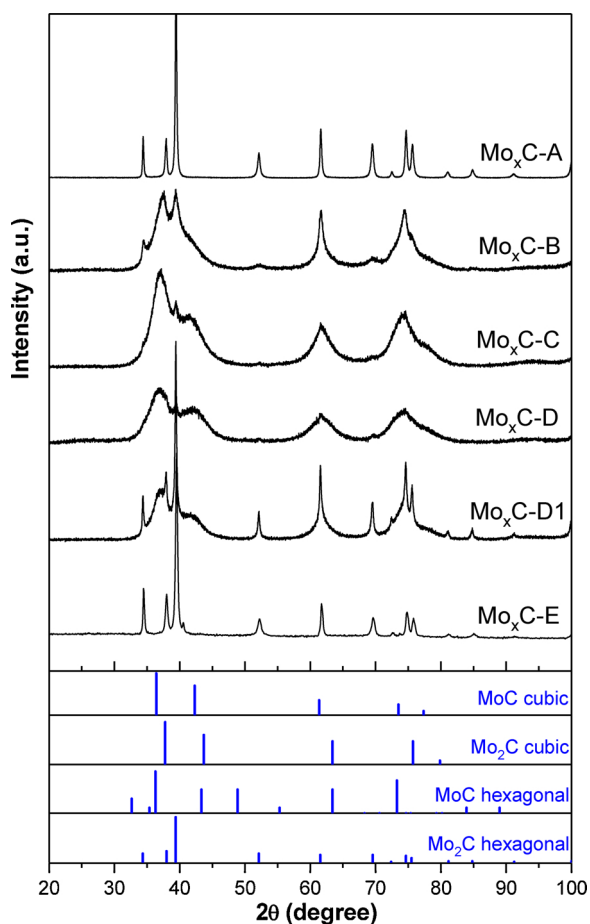


Fig. 1. XRD patterns of Mo_xC catalysts prepared using different methods.

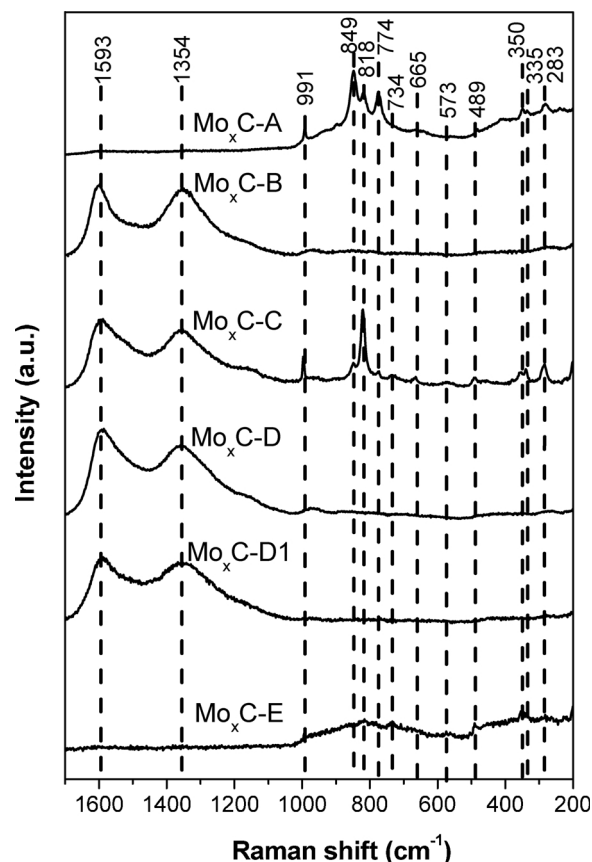


Fig. 2. Raman spectra of Mo_xC catalysts prepared using different methods.

Mo_xC -D and Mo_xC -D1. Moreover, in the pattern of Mo_xC -E, peaks with very low intensity, the most intense at 40.5° , characteristics of Mo^0 (JCPDS 00-042-1120) were found (Fig. 1). From XRD patterns, the presence of crystalline oxycarbide species ($Mo_xO_yC_z$) cannot be ruled out, because only a very small shift on the peak positions of pure Mo_xC phases would be expected when oxycarbide is formed, being the shift a function of the amount of O in the oxycarbide [28,29]. Using the Scherrer equation and the diffraction peak at about $2\theta = 61.6^\circ$, the crystallite sizes of Mo_xC were calculated, which range from 3.3 nm (Mo_xC -D) to 35.2 nm (Mo_xC -A) (Table 1).

Raman spectra were recorded in different zones to determine the presence of molybdenum oxides and/or residual carbon in the catalysts. Except for Mo_xC -A and Mo_xC -E, the presence of two bands at about 1350 and 1580 cm^{-1} (D and G bands) indicate the presence of carbonaceous residues in the catalysts (Fig. 2). The bands in the zone 200–1000 cm^{-1} point to the presence of different surface molybdenum oxide species, mainly MoO_3 , with characteristic Raman bands at about 991, 849, 818, 774, 665, 350, 335 and 283 cm^{-1} ; the small intensity bands at about 734, 573 and 489 cm^{-1} are related to the presence of MoO_{3-x} intermediate oxides [30–35]. The intensity of the bands in the 200–1000 cm^{-1} zone is lower for the Raman spectra corresponding to Mo_xC -B, Mo_xC -D and Mo_xC -D1, indicating the presence of less amount of oxide species on the surface of these catalysts. These species could be formed when Mo_xC catalysts were exposed to air after the preparation [27,36]. A different surface reactivity of the catalysts towards oxygen and mild oxidants is suggested.

Mo_xC -B, which was the most performant catalyst in the RWGS (vide infra), was deeper characterized using SEM-EDX and HRTEM-EELS techniques. Fig. 3A shows the SEM image and the corresponding EDX analysis, which indicates the major presence of Mo and C in the sample and a small amount of O; EDX signals corresponding to N-containing species were not found (see inset in Fig. 3A). A rather wide particle size

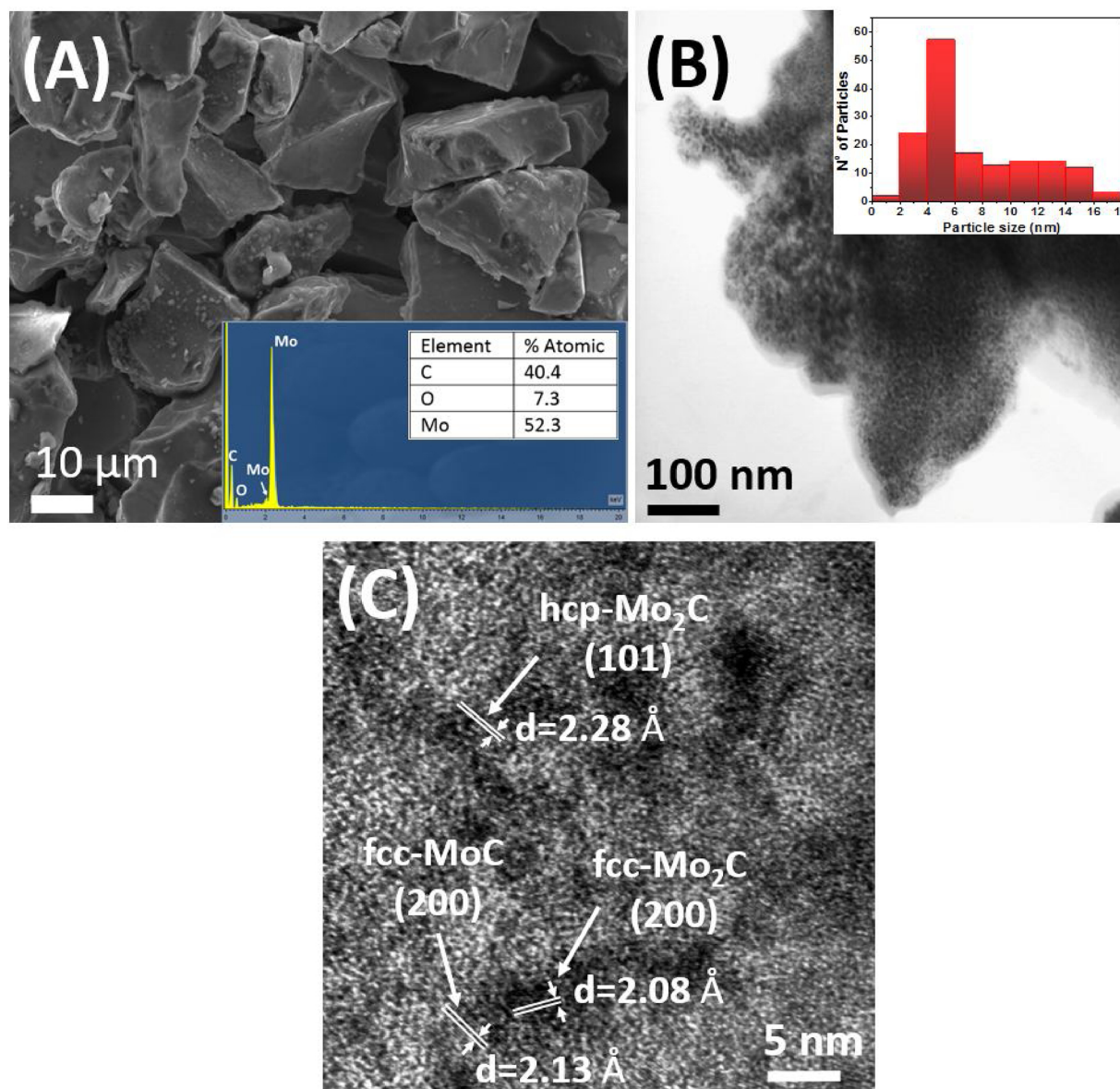


Fig. 3. SEM-EDX and TEM analysis of Mo_xC-B. (A) SEM image and EDX spectrum (inset); (B) TEM image and particle size distribution (inset); (C) HRTEM image.

distribution (2–16 nm) is determined from TEM analysis (inset in Fig. 3B). An HRTEM analysis (Fig. 3C), allowed the identification of nanosized particles of hcp Mo₂C, fcc Mo₂C and fcc MoC phases in this catalyst. Finally the electron energy loss spectroscopy analysis (Fig. S1), confirmed the presence of Mo, C and O in the samples according to EDX results.

Fig. 4 shows the H₂-TPR profiles. All catalysts, showed H₂-consumption peaks below 600 K that can be related with the reduction of Mo_xC_yO_z oxycarbide species that could be formed when catalysts were exposed to air after preparation [27,37]. H₂-TPR peaks in the 600–800 K zone could be related with the reduction of Mo⁵⁺ and/or Mo⁶⁺ in molybdenum oxides. Although peaks over 800 K could be related with the reduction of MoO₂ on the surface of catalysts [27,38], the formation of CH₄ from the residual carbon, which will contribute to the TCD signal cannot be discarded.

C 1s, Mo 3d and O 1s core levels of Mo_xC catalysts were analyzed by XPS. When MoCl₅ was used in the preparation of catalysts (Mo_xC-A and Mo_xC-E), Cl 2p level was also analysed; the absence of Cl 2p signals

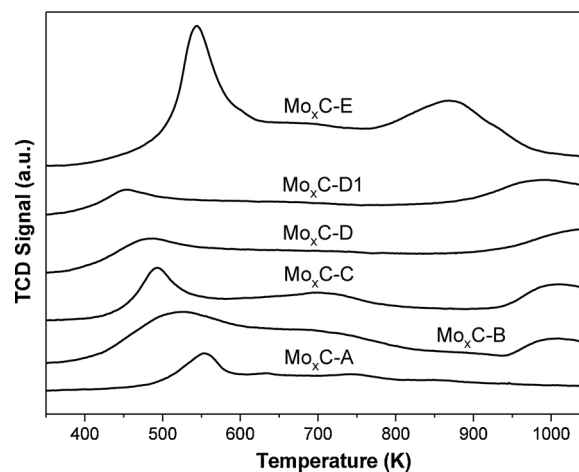


Fig. 4. H₂-TPR profiles of Mo_xC catalysts prepared using different methods.

indicated the absence of residual Cl on the surface of Mo_xC-A and Mo_xC-E. Fig. S2 shows the C 1s and Mo 3d spectra of Mo_xC catalysts. In all cases, C 1s spectra show an intense and asymmetric peak with maximum at 284.8 eV, which can be deconvoluted into four components at 283.4–283.8 eV, 284.8 eV (adventitious carbon), 285.7–286.2 eV and 288.7–289.2 eV (Fig. S2). The component at the lowest BE (283.4–283.8) is related with the presence of Mo-C in molybdenum carbide and/or oxycarbide species, those at higher BE are related to C–O and O=C–O, respectively [39,43]. Although the Mo 3d spectra are complex (Fig. S2), they can be properly deconvoluted into four Mo 3d_{5/2}-Mo 3d_{3/2} doublets with a ratio (intensity Mo 3d_{5/2}/intensity Mo 3d_{3/2}) = 1.5 and a Mo 3d_{5/2}-Mo 3d_{3/2} splitting of 3.1 eV [44]. Mo 3d_{5/2} components at 233.0–233.4 eV, 231.8–232.2 eV and 229.6–230 eV are assigned to Mo⁶⁺, Mo⁵⁺ and Mo⁴⁺ surface species, respectively and are related with the presence of surface oxide molybdenum species [42–44]. The peak at 228.7–228.9 eV can be related to the presence of Mo_xC and/or oxycarbide species [39,43], for Mo_xC-E sample, the intensity of this peak was very low indicating an easier oxidation of the surface species in this case. In all cases O 1s profiles (not shown) showed a main broad and asymmetric peak centred at about 531.1 eV, which can be related to oxide anions in molybdenum oxide and/or oxycarbide species on the surface, shoulders at higher BE are associated to residual species containing C–O and C=O [39–41,43,45].

All catalysts prepared in this work were active and highly selective in the RWGS using a reactant mixture of CO₂/H₂ = 1/3 at 0.1 MPa and 548–673 K; catalytic results are shown in Table 2. As expected, in all cases CO₂ conversion and CO yield increased with the increase of temperature. The main product formed was CO and only small amounts of CH₄, and in some cases negligible amounts of ethylene and propylene, were detected. The CO selectivity values were always higher than 91 %; Mo_xC-B, Mo_xC-D1 and Mo_xC-E showed selectivity to CO always higher than 97 % (Fig. 5). The highest CO production was obtained over Mo_xC-B (Table 2); as stated above, in this catalyst the coexistence of hexagonal Mo₂C and cubic Mo₂C and MoC with poor crystallinity was found; the coexistence of different Mo_xC phases could result in an in-between interface region with enhanced activity. For oxide-supported Cu-based catalysts a main role of the interface region in the RWGS has been reported [46,47]. On the other hand, Mo_xC-A and Mo_xC-E, with only highly crystalline hexagonal Mo₂C as carbide phase, were the less performant catalysts under the reaction condition used.

The apparent activation energy (E_a) for CO production calculated from Arrhenius plots (Fig. S3) in the 598–648 K range, are: Mo_xC-B (37.8 ± 2.4 kJ mol⁻¹) < Mo_xC-D (42.4 ± 1.6 kJ mol⁻¹) < Mo_xC-D1 (45.2 ± 2.3 kJ mol⁻¹) < Mo_xC-E (47.8 ± 0.5 kJ mol⁻¹) < Mo_xC-C (53.7 ± 3.3 kJ mol⁻¹) < Mo_xC-A (56.5 ± 1.5 kJ mol⁻¹). These values compare well with those reported for different metallic- and oxidic-based catalysts for RWGS [48–51]. Mo_xC-A catalyst in which only the presence of hcp-Mo₂C could be identified [27], showed the highest E_a value. It is noticeable the low E_a value (37.8 ± 2.4 kJ mol⁻¹) determined for Mo_xC-B. Mo_xC-B catalyst showed the best performance in

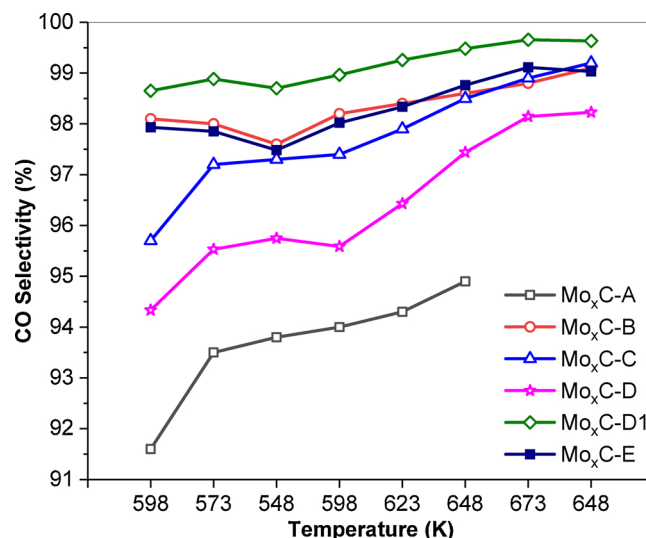


Fig. 5. CO selectivity variation with RWGS temperature for Mo_xC catalysts. Reaction conditions: 150 mg catalyst, CO₂/H₂/N₂ = 1/3/1, GHSV = 3000 h⁻¹, P = 0.1 MPa.

RWGS under the experimental conditions used; an E_a of CO formation of 34 kJ mol⁻¹ has been recently reported for high performant alkali-promoted Pt-based catalysts [50,51]. As discussed above, the ability of CO₂ dissociation into CO and O intermediates and the strength of adsorption on Mo₂C are key points in the RWGS reaction over Mo₂C, and these parameters depend on the exposed Mo₂C surface [27]. One could propose the presence of more surface centres with appropriate characteristics for CO₂ activation and appropriate ability removal of CO and O formed on Mo_xC-B when compared with the other catalysts.

The sequence of temperature carried out in the catalytic test allowed to evaluate the catalytic behaviour at 598 K initially and after about 20 h of catalytic reaction. In all cases, the CO selectivity slightly increased after this time (Fig. 5). Moreover, the CO₂ conversion and CO yield values obtained at 648 K after about 36 h of catalytic test, once the RWGS was studied at 673 K, were very similar to those found at 648 K after about 27 h of reaction (Table 2); the highest decrease of CO₂ conversion and CO yield (≈ 5 %) at 648 K after this sequence was observed for Mo_xC-E. The more performant Mo_xC-B catalyst was tested for about 100 h under the RWGS conditions used in order to verify the stability of its catalytic behaviour. Fig. 6 shows the CO₂ conversion and selectivity to CO along time on stream at 623 K. As can be seen the CO₂ conversion was kept almost constant along the 96 h at about 18 % under RWGS conditions, with a selectivity to CO near to 98 %.

Post-reaction catalysts were analysed by S_{BET}, XRD and Raman spectroscopy. In general, S_{BET} values of post-reaction catalysts were similar to those of fresh samples (Table 1). Except for Mo_xC-E, XRD patterns of post-reaction catalysts did not show significant differences

Table 2

CO yield and CO₂ conversion over Mo_xC catalysts at different temperatures. RWGS reaction conditions: 150 mg catalyst, CO₂/H₂/N₂ = 1/3/1, GHSV = 3000 h⁻¹, P = 0.1 MPa.

T/K	CO yield/mol CO kg _{cat} ⁻¹ h ⁻¹ (% CO ₂ conversion)					
	Mo _x C-A	Mo _x C-B	Mo _x C-C	Mo _x C-D	Mo _x C-D1	Mo _x C-E
598	9.0 (6.0)	18.6 (11.6)	12.2 (7.6)	15.0 (9.7)	13.6 (8.4)	12.0 (7.5)
573	5.6 (3.6)	11.4 (7.1)	6.9 (4.3)	10.1 (6.5)	8.3 (5.1)	6.6 (4.1)
548	2.9 (1.9)	5.8 (3.6)	3.1 (1.9)	5.3 (3.4)	4.0 (2.5)	3.2 (2.0)
598	10.8 (7.0)	18.8 (11.7)	13.1 (8.1)	15.1 (9.7)	14.1 (8.7)	11.5 (7.2)
623	17.4 (11.3)	26.4 (16.4)	21.0 (13.1)	21.8 (13.8)	20.9 (12.9)	17.7 (11.0)
648	25.9 (16.7)	33.8 (21.0)	29.8 (18.5)	29.2 (18.3)	28.4 (17.5)	25.1 (15.5)
673	-	41.8 (25.9)	38.2 (23.7)	36.7 (22.8)	36.2 (22.2)	33.0 (20.3)
648	-	33.6 (20.7)	29.1 (17.9)	29.7 (18.5)	28.6 (17.5)	23.8 (14.7)

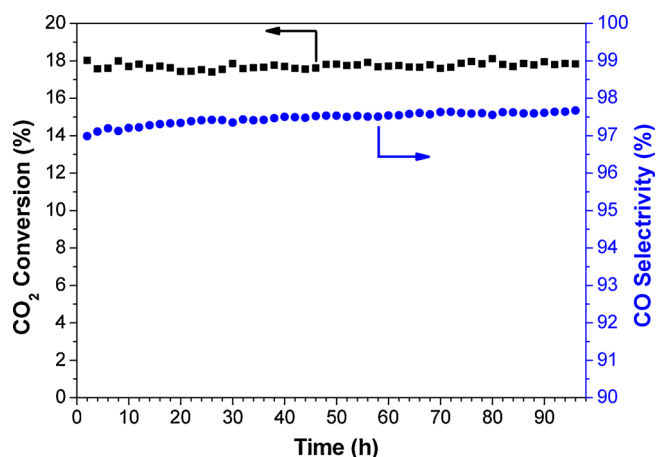


Fig. 6. Catalytic behaviour of Mo_xC-B in RWGS at 623 K as a function of the time on stream: CO₂ conversion and CO selectivity. Reaction conditions: 150 mg catalyst, CO₂/H₂/N₂ = 1/3/1, GHSV = 3000 h⁻¹, P = 0.1 MPa.

with those of fresh catalysts (Fig. S4), being also quite similar the calculated Mo_xC crystallite sizes. Besides the presence of hexagonal Mo₂C and Mo⁰, which were already in fresh Mo_xC-E, XRD pattern of used Mo_xC-E indicates the presence of crystalline MoO₂ (Fig. S4). According with XRD results, Raman analysis of post-reaction Mo_xC-E (Fig. S5) shows a clear increase in the intensity of the bands assigned to molybdenum oxide species with respect those of fresh Mo_xC-E (Fig. 2). Contrarily, Raman spectra of all the other post-reaction catalysts showed bands related with molybdenum oxides with similar or lower intensity than those of the corresponding fresh catalyst.

4. Conclusions

New Mo_xC catalysts were prepared using sol-gel routes and different easy to handle Mo and C precursors, avoiding additional CH₄/H₂ carburization treatments. Mo_xC catalysts were active and selective for the RWGS reaction using CO₂/H₂ = 1/3 mixture in the range 548–673 K at atmospheric pressure. The variation of different parameters in the synthesis, such as the Mo precursor and carbon source, influenced the final characteristics of the Mo_xC catalysts and their catalytic behaviour in RWGS.

Mo_xC-B, Mo_xC-C, Mo_xC-D and Mo_xC-D1 were highly efficient and stable for the CO production under the reaction conditions used. Mo_xC-B which had hexagonal and cubic Mo₂C and MoC phases showed the best catalytic performance. A CO yield of 41.8 mol CO kg_{cat}⁻¹ h⁻¹ was obtained over Mo_xC-B at 673 K with 98.5 % selectivity to CO. A value of E_a for CO production of 37.8 ± 2.4 kJ mol⁻¹ was calculated for Mo_xC-B at 598–648 K.

Acknowledgements

The authors thank MAT2017-87500-P project for financial support. A. P. thanks to MINECO the PhD grant BES-C-2015-074574. X. L. thanks the China Scholarship Council and the University of Barcelona (IN2UB) for her PhD grants. D.J. C.M. is grateful to the European Commission for the scholarship funded within the Erasmus+KA1 Program, ref. 2015-1975/001-001- EMJMD ChIR.

Appendix A. Supplementary data

Supplementary material related to this article can be found, in the online version, at doi:<https://doi.org/10.1016/j.cattod.2019.11.011>.

References

- [1] G. Centi, S. Perathoner, *Catal. Today* 148 (2009) 191–205.
- [2] N. Homs, J. Toyir, P. Ramírez de la Piscina, Catalytic processes for activation of CO₂, in: S.L. Suib (Ed.), *New and Future Developments in Catalysis: Activation of Carbon Dioxide*, Elsevier, Amsterdam, 2013, pp. 1–26.
- [3] Y.H. Choi, Y.J. Jang, H. Park, W.Y. Kim, Y.H. Lee, S.H. Choi, J.S. Lee, *Appl. Catal. B-Environ* 202 (2017) 605–610.
- [4] C.-S. Chen, W.-H. Cheng, S.-S. Lin, *Chem. Commun.* (2001) 1770–1771.
- [5] C.-S. Chen, W.-H. Cheng, S.-S. Lin, *Appl. Catal. A-Gen.* 257 (2004) 97–106.
- [6] X. Su, X. Yang, B. Zhao, Y. Huang, *J. Energy. Chem.* 26 (2017) 854–867.
- [7] M.D. Porosoff, B. Yan, J.G. Chen, *Energy Environ. Sci.* 9 (2016) 62–73.
- [8] L.C. Wang, M.T. Khazaneh, D. Widmann, R.J. Behm, *J. Catal.* 302 (2013) 20–30.
- [9] S.S. Kim, H.H. Lee, S.C. Hong, *Appl. Catal. B-Environ.* 119–120 (2012) 100–108.
- [10] X. Chen, X. Su, H. Duan, B. Liang, Y. Huang, T. Zhang, *Catal. Today* 281 (2017) 312–318.
- [11] S.T. Oyama, *Introduction to the chemistry of transition metal carbides and nitrides*, in: S.T. Oyama (Ed.), *The Chemistry of Transition Metal Carbides and Nitrides*, Springer, Cornwall, 1996, pp. 1–27.
- [12] H.H. Hwu, J.G. Chen, *Chem. Rev.* 105 (2005) 185–212.
- [13] C. Kunkel, F. Viñes, F. Illas, *Energy Environ. Sci.* 9 (2016) 141–144.
- [14] M.D. Porosoff, S. Kattel, W. Li, P. Liu, J.G. Chen, *Chem. Commun.* 51 (2015) 6988–6991.
- [15] H. Tominaga, M. Nagai, *Appl. Catal. A-Gen.* 282 (2005) 5–13.
- [16] J.A. Rodriguez, J. Evans, L. Feria, A.B. Vidal, P. Liu, K. Nakamura, F. Illas, *J. Catal.* 307 (2013) 162–169.
- [17] S. Posada-Pérez, P.J. Ramírez, R.A. Gutiérrez, D.J. Stacchiola, F. Viñes, P. Liu, F. Illas, J.A. Rodriguez, *Catal. Sci. Technol.* 6 (2016) 6766–6777.
- [18] J.S. Lee, S.T. Oyama, M. Boudart, *J. Catal.* 106 (1987) 125–133.
- [19] A. Hanif, T. Xiao, A.P.E. York, J. Sloan, M.L.H. Green, *Chem. Mater.* 14 (2002) 1009–1015.
- [20] M. Patel, J. Subrahmanyam, *Mater. Res. Bull.* 43 (2008) 2036–2041.
- [21] W. Xu, P.J. Ramírez, D. Stacchiola, J.L. Brito, J.A. Rodriguez, *Catal. Lett.* 145 (2015) 1365–1373.
- [22] D. Zeng, M.J. Hampden-Smith, *Chem. Mater.* 4 (1992) 968–970.
- [23] C. Giordano, C. Erpen, W. Yao, M. Antonietti, *Nano Lett.* 8 (2008) 4659–4663.
- [24] A.M. Stux, C. Laberty-Robert, K.E. Swider-Lyons, *J. Solid State Chem.* 181 (2008) 2741–2747.
- [25] L. Zhao, K. Fang, D. Jiang, D. Li, Y. Sun, *Catal. Today* 158 (2010) 490–495.
- [26] G. Vitale, H. Guzmán, M.L. Frauwallner, C.E. Scott, P. Pereira-Almao, *Catal. Today* 250 (2015) 123–133.
- [27] X. Liu, C.R. Kunkel, P. Ramírez de la Piscina, N. Homs, F. Viñes, F. Illas, *ACS Catal.* 7 (2017) 4323–4335.
- [28] P. Delporte, F. Meunier, C. Pham-Huu, Ph. Vennegues, M.J. Ledoux, *J. Guille, Catal. Today* 23 (1995) 251–267.
- [29] Ch. Bouchy, C. Pham-Huu, B. Heinrich, Ch. Chaumont, M.J. Ledoux, *J. Catal.* 190 (2000) 92–103.
- [30] M. Dieterle, G. Mestl, *Phys. Chem. Chem. Phys.* 4 (2002) 822–826.
- [31] M. Dieterle, G. Weinberg, G. Mestl, *Phys. Chem. Chem. Phys.* 4 (2002) 812–821.
- [32] J.V. Silveira, J.A. Batista, G.D. Saraiva, J. Mendes Filho, A.G. Souza Filho, S. Hu, X. Wang, *Vib. Spectrosc.* 54 (2010) 179–183.
- [33] M. Camacho-López, L. Escobar-Alarcón, M. Picquart, R. Arroyo, G. Córdoba, E. Haro-Poniatowski, *Opt. Mater.* 33 (2011) 480–484.
- [34] M.-L. Frauwallner, F. López-Linares, J. Lara-Romero, C.E. Scott, V. Ali, E. Hernández, P. Pereira-Almao, *Appl. Catal. A Gen.* 394 (2011) 62–70.
- [35] T.-C. Xiao, A. Hanif, A.P. York, Y. Nishizaka, M.L. Green, *Phys. Chem. Chem. Phys.* 4 (2002) 4549–4554.
- [36] W. Wu, Z. Wu, C. Liang, P. Ying, Z. Feng, C. Li, *Phys. Chem. Chem. Phys.* 6 (2004) 5603–5608.
- [37] G. Wang, J.A. Schaidle, M.B. Katz, Y. Li, X. Pan, L.T. Thompson, *J. Catal.* 304 (2013) 92–99.
- [38] P. Arnoldy, J.C.M. De Jonge, J.A. Moulijn, *J. Phys. Chem.* 89 (1985) 4517–4526.
- [39] Q. Gao, X. Zhao, Y. Xiao, D. Zhao, M. Cao, *Nanoscale* 6 (2014) 6151–6157.
- [40] Y. Zhu, S. Wang, Y. Zhong, R. Cai, L. Li, Z. Shao, *J. Power Sources* 307 (2016) 552–560.
- [41] Y. Sun, X. Hu, W. Luo, Y. Huang, *J. Mater. Chem.* 22 (2012) 425–431.
- [42] R. Li, S. Wang, W. Wang, M. Cao, *Phys. Chem. Chem. Phys.* 17 (2015) 24803–24809.
- [43] M.D. Porosoff, X. Yang, J.A. Boscoboinik, J.G. Chen, *Angew. Chem.* 126 (2014) 6823–6827.
- [44] K. Oshikawa, M. Nagai, S. Omi, *J. Phys. Chem. B* 105 (2001) 9124–9131.
- [45] M. Chen, J. Liu, W. Zhou, J. Lin, Z. Shen, *Sci. Rep.* 5 (2015) 10389–10399.
- [46] X. Liu, P. Ramírez de la Piscina, J. Toyir, N. Homs, *Catal. Today* 296 (2017) 181–186.
- [47] C. Álvarez Galván, J. Schumann, M. Behrens, J.L.G. Fierro, R. Schlögl, E. Frei, *Appl. Catal. B: Environ.* 195 (2016) 104–111.
- [48] K.-H. Ernst, Ch.T. Campbell, G. Moretti, *J. Catal.* 134 (1992) 66–74.
- [49] M.S. Spencer, *Catal. Lett.* 32 (1995) 9–13.
- [50] B. Liang, H. Duan, X. Su, X. Chen, Y. Huang, X. Chen, J.J. Delgado, T. Zhang, *Catal. Today* 281 (2017) 319–326.
- [51] J.L. Santos, L.F. Bobadilla, M.A. Centeno, J.A. Odriozola, *J. Carbon Res.* 4 (2018) 47–62.